ADVANCED FUNCTIONAL MATERIALS
www.afm-journal.de

Reversible Disorder in a Room Temperature Ferromagnet

*Spencer L. Tomarken, Daniel M. Silevitch, Gabriel Aeppli, Braden A.W. Brinkman, Jian Xu, Karin A. Dahmen, and Thomas F. Rosenbaum**

Random magnetic fields, varying from site to site in a magnetic material, are a form of disorder that can determine the local architecture and stability of the magnetic state. In a ferromagnet, the application of an external magnetic field can amplify the effects of the internal random fields and, in principle, harden a magnetic domain, without changing temperature and only for as long as the external field is present. Here, the rare-earth compound $Nd_2Fe_{14}B$, formed with a granular morphology of random-packed, elongated grains, is an experimental realization of the Random Field Ising Model in a room temperature ferromagnet. The application of magnetic fields transverse to the easy axis tunes the coupling between the structural disorder and the magnetic pinning properties. This material both illuminates the intricacies of tunable disorder and serves as a guidepost along the way to developing increased-density magnetic storage media.

1. Introduction

Disorder is a necessary characteristic of magnetic materials crafted for information storage. Changing the state of a bit involves a delicate competition between the local disorder's propensity to pin the state of the magnetic domain and the ability of thermal fluctuations and applied fields to flip the bit. Material growth conditions most commonly determine the level of disorder in a storage medium. For example, varying the argon pressure in sputter-deposited thin film magnets changes the growth kinetics, leading to particular morphologies with attendant degrees of order.[1,2] The limitation of such approaches, however, is that variations in the local potential are literally baked into each sample at the time of growth. It is possible in principle to overcome this obstacle by using materials that are realizations of the Random Field Ising Model (RFIM).[3–5] The strength of pinning centers created by local random fields can be tuned by an external magnetic field, thereby creating a magnet in which the degree of disorder can be continuously and reversibly varied. Up to now, the only physical realizations of the RFIM have been in antiferromagnets and in ferromagnets with Curie temperatures near absolute zero. We describe here a technique to stabilize RFIM ferromagnetism at room temperature and above, providing a test bed for domain dynamics in a tunable potential and opening the door to possible applications. Additionally, we report simulation results that provide the first known numerical substantiation of a physical realization of the ferromagnetic RFIM.

For more than 30 years, a host of different materials have been studied as experimental realizations of the field-tuned RFIM. The initial realizations, site-diluted antiferromagnets,[3,6] opened the door for extensive work on the critical behavior and dynamics[7,8] of the RFIM, but the absence of a net moment limited the tools that could be applied. Within the last decade, it has been shown that dilute dipole-coupled ferromagnets also can exhibit RFIM behavior. The combination of off-diagonal components in the dipole-dipole coupling term and the breaking of translational invariance due to random dilution leads to an effective random field whose strength can be tuned continuously via a uniform magnetic field applied transverse to the Ising axis.[9–11] Experimental realizations have been observed in the dilute rare-earth fluoride $LiHo_xY_{1-x}F_4$[10] and the molecular magnet Mn_{12}-acetate;[12] see **Figure 1** of Ref. [10] and Figure 4 of Ref. [12] for qualitative illustrations of how random fields arise in a transverse field Ising model. Moreover, the presence of tunable random fields can be exploited to vary isothermally the pinning energies and domain dynamics of the magnet, creating a system that can be switched at fixed temperature between magnetically hard and soft reversal modes.[13] While both materials exhibit field-induced quantum fluctuations, the transverse field scales for such fluctuations exceed those necessary to observe random-field effects.[12,13] Unfortunately, both materials are only ferromagnetic at temperatures below 1 K due to the intrinsically small energy scale of the single-spin dipole–dipole coupling.[10,12] Technological interest awaits the discovery of random-field tuning at room temperature.[14]

2. Results and Discussion

For dipole-coupled ferromagnets to be stable at elevated temperatures, the individual dipoles must have moments two to

S. L. Tomarken, Dr. D. M. Silevitch, J. Xu, Prof. T. F. Rosenbaum
The James Franck Institute and Department of Physics
The University of Chicago
929 E. 57th Street, Chicago, Illinois, 60637, USA
E-mail: tfr@uchicago.edu
Prof. G. Aeppli
Department of Physics & Astronomy and London Center for Nanotechnology
University College London
London, WC1E 6BT, UK
B. A. W. Brinkman, Prof. K. A. Dahmen
Department of Physics
University of Illinois at Urbana-Champaign
Urbana, Illinois, 61801, USA

DOI: 10.1002/adfm.201303231

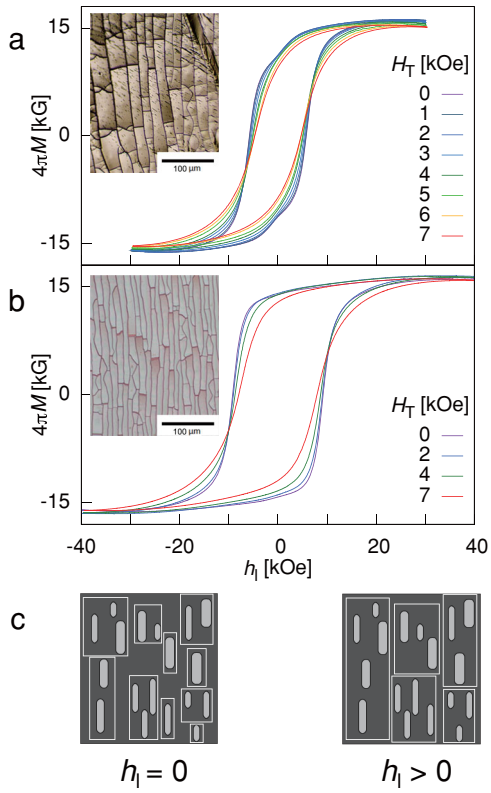

Figure 1. Overview of magnetic behavior of $Nd_2Fe_{14}B$ samples A and B. a,b) Magnetic behavior and structural morphology of two samples of $Nd_2Fe_{14}B$. Main panels: Magnetic hysteresis loops at T = 300 K for a series of transverse magnetic fields. Loops are swept out at a constant ramp of 0.75 kOe/min along the longitudinal (easy) axis while keeping the transverse field fixed. At low (high) longitudinal field, application of a transverse field narrows (broadens) the hysteresis. Insets: Optical micrographs of the $Nd_2Fe_{14}B$ samples' grain structure using dried ferrofluid as a fine-powder contrast-enhancing agent that preferentially settles in the grain boundaries. The magnetic easy axis is in the vertical direction. a) The granular structure is polydisperse in both size and aspect ratio, leading to a clear separation of the high and low field regimes. b) The granular structure consists almost entirely of elongated aspect ratio grains, yielding a squarer hysteresis loop for low transverse fields. In both samples, the grains are tightly packed with little interstitial volume. c) Schematic of magnetic grain coarsening with longitudinal field. As the longitudinal field increases, coarsening effects increase the average size of the magnetic domains, which can span several structural grains and can average out the intergrain disorder.

three orders of magnitude larger than the single-ion moments of the $Li(Ho,Y)F_4$ or Mn_{12}-acetate systems. We satisfy this fundamental constraint by considering a rare-earth ferromagnet, $Nd_2Fe_{14}B$, with high crystalline anisotropy and a tendency to form elongated grains.[15] The behavior of the magnet as a whole effectively separates into two length and energy scales: domains within a single grain and interactions between grains. At the smallest length scales, the individual spins are exchange-coupled, yielding a Curie temperature of 585 K.[16] At zero applied field they form domains whose size can be estimated from the known anisotropy energies and saturation magnetization to be of order 0.2–0.3 μm.[17] This yields a typical net moment of order 10^9 Bohr magnetons and an interdomain dipole interaction energy of approximately 5 k_BT at 300 K.[18] Due to the crystalline and shape anisotropy,[19,20] each grain ultimately acts like a single effective spin that couples to nearby grains via the dipolar interaction (the long range nature of the dipole interaction results in a coupling that extends beyond nearest neighbors). While this energy scale is large compared to typical magnetic storage media, the results reported here represent a proof of concept that RFIM effects can be used to tune the behavior of room temperature ferromagnets. This ensemble of grains with typical size (50 mm × 15 mm × 15 mm) mimics the collection of individual dipoles in the previously studied RFIM materials and may be expected to exhibit comparable behavior. The large-scale grain structure can be imaged directly (Figure 1a,b insets), where a dried ferrofluid that accumulates at the grain boundaries serves to enhance the contrast (see Experimental Section). As can be seen from the two samples shown in Figure 1, the grains are randomly packed in the material with the long axis of the majority of grains oriented parallel to the bulk easy axis of the sample (vertical in Figure 1); Sample A contains approximately 60% elongated grains by volume and Sample B contains approximately 96%. This random packing is key to the observation of the RFIM, as the random distribution breaks the translational symmetry which otherwise would result in a net cancellation of the off-diagonal terms in the dipole-dipole interaction tensor. Random packing of dipoles is known under some circumstances to destroy the long-range ordered state and instead create a glass state with no net magnetization.[21] However, the large remnant magnetization observed in this case (~75% and ~86% of M_s for $H_T = 0$ for samples A and B in Figure 1a and 1b, respectively) demonstrates that this sample has sufficiently high density and low frustration to support an ordered ferromagnetic state.[22]

As a longitudinal field h_l is applied and the magnetic domains are aligned, the effects of disorder and pinning change. Starting in the limit of high longitudinal field, defined when the magnet is near saturation, the average domain size approaches the dimensions of the sample. As sketched in Figure 1c, there are only a few, large domains due to the nearly uniform ordering of magnetic grains parallel to the applied field. With reduced longitudinal field, new domains nucleate within the material and the average domain size eventually becomes small compared to the typical grain size of order 10 μm.[23] During magnetization reversal, domain wall pinning occurs between the grains and material defects within the sample,[24] fixed at fabrication. The number of such pinning sites a propagating domain wall encounters is proportional to the surface area of the wall; by contrast, the magnetic moment of the domain is proportional to the volume. Hence, at high longitudinal field where there are a small number of big domains, the effective strength of the pinning is weaker than at low longitudinal field, where the higher surface area to volume ratio of the smaller domains results in stronger effective pinning.

We plot in the main panels of Figure 1a,b magnetic hysteresis loops for both samples as a function of h_l beyond saturation (±25 kOe) at a series of constant transverse fields, H_T. The saturation magnetization in the longitudinal direction is only weakly dependent on H_T, decreasing by 3% (A) and 2% (B) at 7 kOe of transverse field and quantitatively consistent with the tilting of a small fraction of the spins into the transverse plane.

The small deviations from pure Ising behavior due to finite anisotropy demonstrate that the predominant effect of the transverse field is to create a site random field in the longitudinal direction. The evolution of the shape of the hysteresis loops as a function of H_T is more complex. The shoulder visible at low transverse field at $h_l \sim 3$ kOe in sample A along with the meeting of all of the curves at $h_l \sim 7$ kOe ($h_l \sim 10$ kOe for sample B) suggest that there are two regimes which should be considered separately; for $h_l < 7/10$ kOe, the loops narrow as the transverse field is increased, while above 7/10 kOe, the application of a transverse field actually broadens the hysteresis loops. Broadening, defined from the integrated area of the loops, cannot be explained by a simple coarsening of the domains or rotation of the spins as both effects act to decrease the stored energy of a ferromagnet and narrow the hysteresis loop.

Instead, one must consider the dominant interactions that impede magnetization reversal in high anisotropy magnetic systems. Nucleation tends to enhance magnetization reversal while domain wall pinning serves to impede magnetization reversal. Whether or not a defect will contribute to nucleation or pinning is dependent on the defect's tendency to either raise or lower the local magnetic anisotropy as well as the defect demagnetization field.[25] We note that in uniaxial ferromagnets grain boundaries are known to be particularly effective sources of domain wall pinning.[25] Furthermore, in $Nd_2Fe_{14}B$ samples synthesized with similar high-anisotropy microstructures, domain wall pinning has been shown to dominate the magnetization reversal mechanism.[26] We conclude that the broadening of the hysteresis loops with transverse field in the high longitudinal field regime arises from increased domain wall pinning, and note the absence of any other mechanisms for broadening identified in the literature.

Due to the more clearly defined separation between the different field regimes and for the sake of clarity, we describe the behavior of sample A alone in fuller detail. We plot in **Figure 2** a series of nested subloops for both $H_T = 0$ (Figure 2a,c,e) and 6 kOe (Figure 2b,d,f) in order to illuminate the underlying mechanisms in the different longitudinal field regimes, The subloops allow us to explore the energy hierarchies that form during nested longitudinal field trajectories. Each measurement starts at sufficiently high longitudinal field to saturate the magnetization along the applied field, followed by a ramp down to the starting field of the subloop sequence. The longitudinal field is then adiabatically ramped through a series of nested subloops (with the maximal h_l decreasing by a fixed amount per subloop, typically 1 kOe per subloop) that cover either the low or high longitudinal field ranges. As the subloop series progresses, the sample converges on its equilibrium magnetization, and the series of nested loops corresponds to a hierarchy of energies at each "turning point".[27]

The subloops in the low longitudinal field regime (Figure 2e,f) narrow as the transverse field is applied, reflecting a decrease in the barriers to domain movement and consistent with the behavior of the full hysteresis loops shown in Figure 1a. In contrast, subloops in the high longitudinal field regime (Figure 2c,d) broaden with application of a transverse field indicating an enhancement of domain wall pinning, also in agreement with Figure 1a. Next we compare and contrast the evolution of the four subloop sets as they are driven through a nested set of field sweeps. Consider the low longitudinal subloop sets (Figure 2e,f). With respect to the outermost subloop, the interior subloops scale inwards and form new $M(h_l)$ trajectories that do not overlay with the initial outermost subloop in both the $H_T = 0$ and 6 kOe runs. We contrast this evolution with the behavior of the nested subloops at high longitudinal field (Figure 2c,d). In the $H_T = 0$ case, the subloops fail to depart from the original outermost subloop (loop number 1 in Figure 2c). The interior trajectories all overlay this initial outer trajectory. With application of a 6 kOe transverse field we depart from this striking collapse and observe that interior subloops leave the outermost subloop and form unique $M(h_l)$ trajectories nested within the outermost subloop.

In order to connect these results to theory, we rely on the results of computer simulations of hysteresis subloops in both

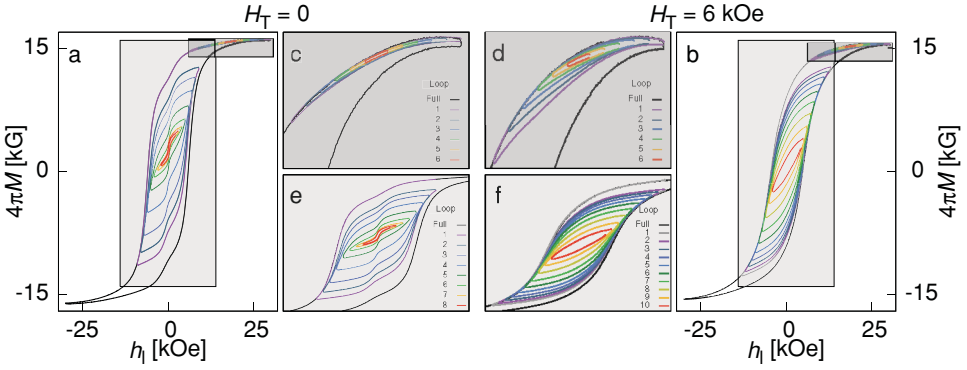

Figure 2. Effects of transverse field on subloop evolution. a,b) Series of nested subloops (colored) inside overall hysteresis loops (black) at $H_T = 0$ (a) and $H_T = 6$ kOe (b). c,d) Nested subloops at high longitudinal field (centered on $h_l = 18.5$ kOe, with loop #1 ranging from 30 to 7 kOe, loop #2 ranging from 29 to 8 kOe, and following that sequence through the final loop which ranges from 20 to 17 kOe). e) Nested low longitudinal field subloops at $H_T = 0$, starting at loop #1 with $|h_l| = 9$ kOe and decreasing for subsequent loops in maximum field by 1 kOe per loop, ending at $|h_l| = 3$ kOe. f) Nested low longitudinal field subloops at $H_T = 6$ kOe, starting at loop #1 with $|h_l| = 13$ kOe and decreasing for subsequent loops in maximum field by 1 kOe per loop, ending at $|h_l| = 5$ kOe. In the $H_T = 0$ regime, the high longitudinal field subloops (c) retrace the original outermost subloop (loop #1) unlike the low longitudinal field subloops (e,f), indicating relatively weak disorder. In the $H_T = 6$ kOe regime, the high longitudinal field subloops (d) deviate from the outermost subloop, indicating strong effective disorder.

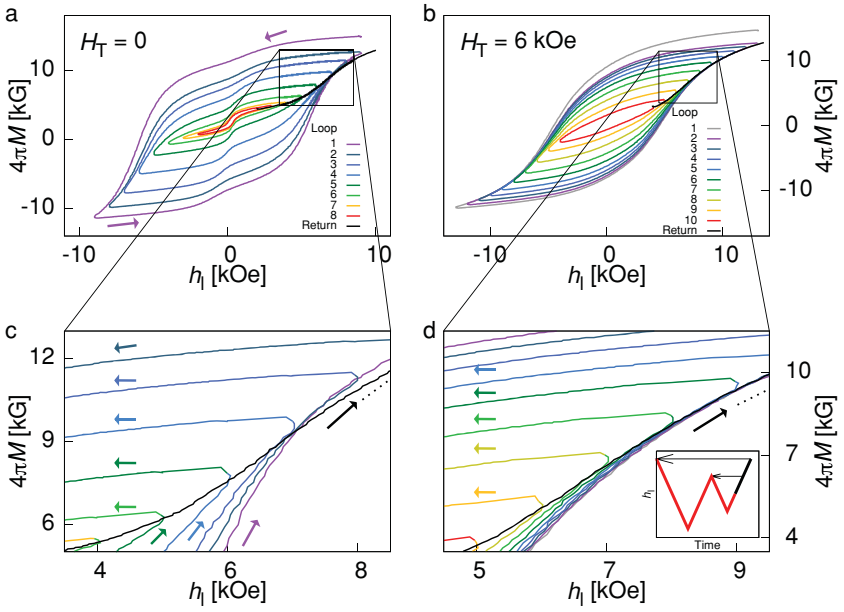

Figure 3. Transverse-field assisted return point memory. a,c) Return point memory in the absence of a transverse field. The longitudinal field is ramped in a decreasing triangle pattern, with $|h_l|$ starting at 9 kOe for loop #1 and decreasing by 1 kOe per subsequent subloop, followed by a linear ramp back up to saturation as sketched in the inset. Return point memory, a characteristic signature of strong disorder, fails at h_l = 7 kOe, as seen by the crossing of the return line (black) through the original subloops (colored). b,d) Return point memory is stable in a transverse field of 6 kOe. The longitudinal field is ramped in a set of nested subloops starting with loop #1 at $|h_l|$ = 13 kOe and decreasing by 1 kOe steps per subloop to $|h_l|$ = 5 kOe, followed by a ramp back up to 30 kOe. Arrows show direction of field ramping along the subloop sequence and subsequent return to large longitudinal field. Inset: Schematic of return point memory. On the return path to saturation, the system retains memory of past magnetization extrema.

the small and large randomness limit of the ferromagnetic RFIM.[27] These simulation results show that for small values of randomness below a critical threshold, hysteresis subloops collapse onto the same overall outer subloop trajectory in a manner qualitatively consistent with our Figure 2c. Subloops above the critical threshold of randomness are seen to scale inwards in a manner qualitatively similar to both the low longitudinal field subloop sets (Figure 2e,f) as well the H_T = 6 kOe high longitudinal field subloop set (Figure 2d). The simulations support the claim that the low longitudinal field regime is in a strongly disordered regime, while the high longitudinal field regime experiences intrinsically weak disorder due to the weakened effect of domain wall pinning. The application of a strong transverse field with a concomitant increase in local random fields and pinning of domain walls serves to capture the characteristics of the strongly disordered state.

The sharp steps in the magnetization that occur in the smallest low-field subloops for H_T = 0 (Figure 2e) point to a small volume fraction of the sample exhibiting magnetically soft behavior with switching fields of order 1 kOe (in agreement with our observation of a few percent reduction in the remnant magnetization at 6–7 kOe transverse field). This behavior can arise from a small number of grains of appropriate size and shape to be only weakly coupled to their neighbors, and thereby can easily rotate their magnetization to track the applied field. The disappearance of these low-field features upon application of a transverse field (Figure 2f) is consistent with this interpretation, as the moments of these grains would simply rotate towards the transverse direction at low longitudinal fields and decrease their contribution to the longitudinal magnetization.

We pursue our interrogation of the relationship between transverse field, disorder, and domain dynamics through the method of return point memory (RPM).[28] RPM is the ability of the material to arrive at the same microscopic configuration independent of the specific applied field path. Specifically, in a material possessing RPM, two independent applied field paths (not necessarily monotonic) with identical endpoints will arrive at the same microscopic configuration provided neither path exceeds the endpoint applied field values at any interior point of the trajectory.[28–30] In the context of the hysteresis subloops of Figure 2, each subloop has a maximum and minimum applied field value by construction. Within a given subloop, all interior subloops form trajectories that are nested within the (outer) subloop boundaries. Sets of nested subloops provide a natural construct to test the existence of RPM because each interior subloop respects these basic boundary conditions with respect to all outer subloops, creating a hierarchy of microstates which must be remembered if RPM holds. Because RPM is solely a property of hard (as opposed to soft) magnets, it provides a powerful probe of whether a given system is in a strongly disordered state such as a random-field-dominated regime.[28]

We test return-point memory in **Figure 3** in the absence (a,c) and presence (b,d) of a transverse field. The field trajectory followed in the RPM measurements is sketched in the inset to Figure 3d. At constant H_T, the longitudinal field is cycled back and forth with the magnitude decreasing by 1 kOe per cycle, similar to the nested subloop measurements described above. The series of nested subloops forms a hierarchy of turning points at the end of each subloop. After the final cycle, h_l is smoothly ramped back up to the initial saturation value. In a material exhibiting RPM, whenever the return field matches the applied field of one of the turning points, the magnetizations will be equivalent (arrows in the inset), and the return path should intersect the hysteresis subloops at and only at each subloop endpoint.[29]

Without the application of a transverse field, RPM breaks down above h_l = 7 kOe as the return curve falls below the original subloops (Figure 3c). As h_l increases, characteristic domain sizes grow, spanning multiple grains, and the effects of the intrinsic disorder become proportionally weaker, leading to a loss of memory. Remarkably, a transverse field restores RPM. With H_T = 6 kOe, return point memory persists throughout the entire longitudinal field range (Figure 3b,d), as indicated by the return path not crossing the original set of subloops.

ADVANCED FUNCTIONAL MATERIALS
www.afm-journal.de

www.MaterialsViews.com

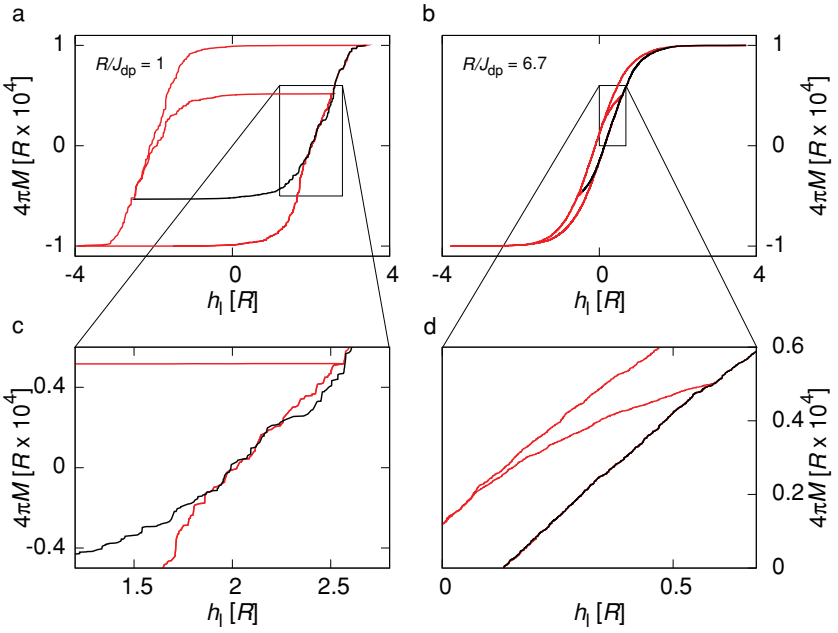

Figure 4. Computer simulations of Return Point Memory for the RFIM with dipolar interactions. a,c) Return point memory in the low random field regime (relative to the strength of the dipolar coupling) with applied field and magnetization in units of the randomness, R. b,d) Return point memory in the high random field regime (relative to the strength of dipolar coupling). Both limits are consistent with the data for $Nd_2Fe_{14}B$ in Figure 3.

The random fields induced by the transverse field at each grain boundary have increased the pinning potential to the point where the material remains in the strong-disorder limit up to magnetization saturation. In particular, the presence of return-point memory in this system demonstrates that the effects of the random fields dominate over the diagonal terms of the dipole-dipole interaction, as RPM is only manifest in the strong-disorder limit.[30] In light of the RPM results, we can return to the hysteresis loops presented in Figure 1a and note that at low transverse field the randomness-dominated regime at low longitudinal field evolves into a weakly disordered regime at high field, with a plateau-like crossover region at $h_l \sim 7$ kOe. At high fixed transverse fields, the enhancement of the random field effects means that the strong randomness regime persists to much larger longitudinal fields, eliminating the crossover region. While the transverse field was only applied in one direction in the transverse plane, it is expected that results would be similar for other transverse orientations.

Simulations of the non-equilibrium, zero-temperature Random Field Ising Model[31–34] with dipolar couplings substantiate this picture (**Figure 4**). Here, 10^4 spins (grains) on a 50×200 size, two-dimensional lattice (which mimics the essential geometric features of the $Nd_2Fe_{14}B$ sample) flip as each spin's effective local field changes sign. The local field incorporates the sum of the slowly varying external longitudinal magnetic field, the dipolar field, and the random field at each spin site. The relative strength of the randomness is captured by varying the ratio of the random field to the strength of the dipolar interaction.

The sample grains are modeled as coarse-grained spins that interact with each other via dipolar forces; exchange couplings between the grains are found to be very weak. The grains interact with an external magnetic field with both longitudinal and transverse components. The grains align with the longitudinal field and the transverse field generates effective longitudinal random fields at each site, similar to the effective random fields in $LiHo_xY_{1-x}F_4$. The dynamics are thus described by the Hamiltonian in Equation (1):

$$H = -\sum_{ij} J_{ij} s_i^z s_j^z - \sum_i (H^z(t) + h_i^z) s_i^z \quad (1)$$

Here, s_i^z is a classical spin, at site i in the z direction, with possible values of ±1, J_{ij} is a purely dipolar interaction between spins i and j with no exchange interactions (see Equation (2) below), $H^z(t)$ is a longitudinal field, and h_i^z is a local longitudinal random field at site i. The first sum is performed over all pairs (i,j), and is not restricted to nearest neighbors. We assume that the random fields follow a normal distribution of variance R^2. This variance characterizes the "disorder" of the system, as there is little spread in random fields for small R and a large spread for larger R. We will henceforth refer to R as the "disorder." By contrast, in the actual experiment, the disorder is tuned by adjusting the strength of the transverse magnetic field.

The form of the dipolar interaction depends on the dimension and alignment of our system. Although our system is cylindrical in shape, because the length of the sample is much longer than its diameter, we expect that a rectangular Ising model simulation will be sufficient to capture the qualitative behavior of the experiment. In particular, we are primarily interested in the behavior of the return-point-memory as the strength of the disorder is varied relative to the strength of the dipolar interactions. The form of the dipolar interaction in this case is given by Equation (2):

$$J_{ij} = J_{dp} \frac{3(\cos\theta_{ij})^2 - 1}{r_{ij}^3}, \quad (2)$$

where θ_{ij} is the angle between spins i and j, r_{ij} is the distance between the spins, and J_{dp} is the strength of the dipolar interaction. Note that the overall sign of J_{ij} may be positive or negative.

The system is initialized with the longitudinal field $H^z(t)$ at a sufficiently large negative value to force all spins to point down. Each spin aligns with its effective local field, $s_i = \mathrm{sgn}(h^{eff}_i)$, where the local field is described by Equation (3):

$$h_i^{eff}(t) = h_i + \sum_j J_{ij} s_j^z + H^z(t). \quad (3)$$

Each spin flip can increase or decrease the effective field of every other spin, and may change their effective local fields, causing other spins to flip, resulting in an avalanche of spin flips. We increase $H^z(t)$ adiabatically, such that the increase of the field does not proceed faster than the propagation of an

avalanche. To achieve this in practice, we compute the value of $H^z(t)$ necessary to trigger a spin to flip, and increase it to that value. We then hold $H^z(t)$ fixed while the avalanche propagates. When the avalanche ends, we compute the value of $H^z(t)$ needed to start the next avalanche. We continue in this way until all spins point up. At this point, we repeat the procedure sweeping down. In order to investigate subloops, we switch the direction of our sweep before the system reaches saturation.

We perform similar simulations for several ratios of R/J_{dp} in order to investigate the behavior of the return point memory at large transverse fields (large R) versus small transverse fields (small R). Rather than generate a new set of random fields for every simulation, we draw the random fields from a standard normal distribution and adjust the strength of the dipolar interactions. As the dipole coupling and the random fields are the only coupling scales in the simulation, the results depend on the ratio of the two quantities and hence this procedure (chosen for computational efficiency) is equivalent to regenerating the random fields.

The simulations capture the salient features of the experiment. As seen in Figure 4a,c, in the weak-random field regime the subloops do not join back up with the original loops to retrace the path back to magnetic saturation, signaling an absence of RPM at higher longitudinal field. This corresponds to the data for $Nd_2Fe_{14}B$ in Figure 3a,c that display a failure of return point memory for $h_l > 7$ kOe. The simulations demonstrate the restoration of RPM in the strong random field regime (Figure 4b,d), consistent with the effects of the transverse field in Figure 3b,d.

3. Conclusions

Experiments and computer simulations thus support the supposition that uniaxial grains in a common rare-earth ferromagnet behave as effective Ising dipoles, renormalizing the energy scale to room temperature and above. A transverse field can isothermally tune the pinning potential for magnetic domains from the weak disorder to the strong disorder limit. In the context of magnetic storage, this would allow entering a soft state for writing and switching to a hard reversal mode with a larger reversal energy for long-term retention and reading.[35] Readily available, tunable random-field ferromagnets also would open up experimental studies of theoretical and computational predictions for the behavior of the RFIM. This would include the dynamics and distribution of avalanches during reversal, which should be accessible via Barkhausen noise techniques.

4. Experimental Section

We studied the magnetization behavior of nominally-equivalent commercial $Nd_2Fe_{14}B$ magnets (McMaster-Carr) consisting of a set of grains with distributions in length, width, and aspect ratios of (35 ± 25 μm, 18 ± 6 μm, 2 ± 1) (Figure 1a) and (80 ± 50 μm, 12 ± 3 μm, 6 ± 4) (Figure 1b), sintered into a 2 mm diameter × 10 mm length cylinder with the magnetic easy axis parallel to the long axis of the cylinder. The tails of the distributions dominate the differences in the magnetic responses for the two samples. Optical imaging to reveal the shape of the large-scale granular structure followed polishing of the sample to an optical flat and decoration by depositing a commercial colloidal-suspension ferrofluid (Ferrotec EMG 308) and evaporating the liquid. The ferrofluid preferentially settles at the grain boundaries and enhances the contrast. We measured the room temperature magnetization along the easy axis using a pair of passive GaAs Hall sensors (Toshiba THS118) in a gradiometer configuration. The saturation magnetization of 32.2 ± 0.1 m_B per formula unit for both samples indicates that the sintered samples are 99% magnetically dense. The samples and magnetometers were mounted in a vacuum insert placed in the liquid helium bath of a dual-axis 5T/2T superconducting magnet that provided field in the longitudinal (easy) and transverse (hard) directions. A PID feedback loop maintained a constant sample temperature of 300 K during all measurements. Hysteresis loops and nested subloop sets were performed by setting the transverse field at the desired value, waiting for equilibration, and then ramping the longitudinal field in a triangle wave pattern. The longitudinal field was swept at rates ranging from 0.1 to 1.0 kOe/min, with no rate-dependent behavior observed in that range. The computer simulations were performed in an incremental adiabatic limit by increasing the external field the minimum amount necessary to induce the most unstable spin in the system to flip, causing a cascade of spin flips that ends when the entire system of spins reaches a new (meta)stable configuration.

Acknowledgments

The work at The University of Chicago was supported by DOE Basic Energy Sciences Grant No. DE-FG02-99ER45789 and in London by the UK Engineering and Physical Sciences Research Council.

Received: September 18, 2013
Revised: November 17, 2013
Published online: January 23, 2014

[1] M. S. Pierce, C. R. Buechler, L. B. Sorensen, J. J. Turner, S. D. Kevan, E. A. Jagla, J. M. Deutsch, T. Mai, O. Narayan, J. E. Davies, K. Liu, J. H. Dunn, K. M. Chesnel, J. B. Kortright, O. Hellwig, E. E. Fullerton, *Phys. Rev. Lett.* **2005**, *94*, 017202.
[2] M. S. Pierce, C. R. Buechler, L. B. Sorensen, S. D. Kevan, E. A. Jagla, J. M Deutsch, T. Mai, O. Narayan, J. E. Davies, K. Liu, G. Zimanyi, H. Katzgraber, O. Hellwig, E. E. Fullerton, P. Fischer, J. B. Kortright, *Phys. Rev. B* **2007**, *75*, 144406.
[3] S. Fishman, A. Aharony, *J. Phys. C: Solid State Phys.* **1979**, *12*, L729.
[4] E. Pytte, Y. Imry, D. Mukamel, *Phys. Rev. Lett.* **1981**, *46*, 1173.
[5] A. J. Bray, M. A. Moore, *J. Phys. C: Solid State Phys.* **1985**, *18*, L927.
[6] H. Yoshizawa, R. Cowley, G. Shirane, R. Birgeneau, *Phys. Rev. B* **1985**, *31*, 4548.
[7] T. Nattermann, I. Vilfan, *Phys. Rev. Lett.* **1988**, *61*, 223.
[8] R. Bruinsma, G. Aeppli, *Phys. Rev. Lett.* **1984**, *52*, 1547.
[9] S. Tabei, M. Gingras, Y.-J. Kao, P. Stasiak, J.-Y. Fortin, *Phys. Rev. Lett.* **2006**, *97*, 237203.
[10] D. M. Silevitch, D. Bitko, J. Brooke, S. Ghosh, G. Aeppli, T. F. Rosenbaum. *Nature* **2007**, *448*, 567.
[11] M. Schechter, *Phys. Rev. B* **2008**, *77*, 020401.
[12] B. Wen, P. Subedi, L. Bo, Y. Yeshurun, M. Sarachik, *Phys. Rev. B* **2010**, *82*, 014406.
[13] D. M. Silevitch, G. Aeppli, T. F. Rosenbaum, *Proc. Natl. Acad. Sci. USA* **2010**, *107*, 2797.
[14] D. A. Thompson, J. S. Best, *IBM J. Res. Development* **2000**, *44*, 311.
[15] A. Hütten, *JOM* **1992**, *44*, 11.
[16] J. F. Herbst, *Rev. Mod. Phys.* **1991**, *63*, 819.

[17] D. Weller, A. Moser, L. Folks, M. E. Best, W. Lee, M. F. Toney, M. Schwickert, J. U. Thiele, M. F. Doerner, *IEEE Trans. Magn.* **2000**, *36*, 10.
[18] K. D. Durst, H. Kronmüller, *J. Magn. Magn. Mater.* **1987**, *68*, 63.
[19] D. Givord, H. S. Li, R. Perrier de la Bâthie, *Sol. Stat. Commun.* **1984**, *51*, 857.
[20] J. F. Herbst, J. J. Croat, F. E. Pinkerton, W. B. Yelon, *Phys. Rev. B* **1984**, *29*, 4176.
[21] G. Ayton, M. Gingras, G. Patey, *Phys. Rev. E* **1997**, *56*, 562.
[22] T. Miyazaki, H. Jin, The Physics of Ferromagnetism, Springer-Verlag, Berlin, Germany **2012**, p. 100.
[23] J. M. D. Coey, K. O'Donnell, *J. Appl. Phys.* **1997**, *81*, 4810.
[24] D. A. Huse, C. L. Henley, *Phys. Rev. Lett.* **1985**, *54*, 2708.
[25] J. D. Livingston*J. Appl. Phys.* **1981**, *52*, 2544.
[26] J. K. Mishra, *J. Appl. Phys.* **1987**, *62*, 967.
[27] J. H. Carpenter, K. A. Dahmen, J. P. Sethna, G. Friedman, S. Loverde, A. Vanderveld, *J. Appl. Phys.* **2001**, *89*, 6799.
[28] J. Sethna, K. A. Dahmen, S. Kartha, J. A. Krumhansl, B. W. Roberts, J. D. Shore, *Phys. Rev. Lett.* **1993**, *70*, 3347.
[29] J. Deutsch, A. Dhar, O. Narayan, *Phys. Rev. Lett.* **2004**, *92*, 227203.
[30] D. Dhar, P. Shukla, J. P. Sethna, *J. Phys. A: Math. Gen.* **1999**, *30*, 5259.
[31] I. Dayan, M. Schwartz, A. P. Young, *J. Phys. A: Math. Gen.* **1999**, *26*, 3093.
[32] M. Newman, B. Roberts, G. Barkema, J. P. Sethna, *Phys. Rev. B* **1993**, *48*, 16533.
[33] J. P. Sethna, K. Dahmen, O. Perkovic, in *The Science of Hysteresis: Volume II* (Eds: G. Bertotti, I. D. Mayergoyz), Elsevier, Oxford, UK **2006**, pp. 107–180.
[34] J. Carpenter, K. Dahmen, A. Mills, M. Weissman, A. Berger, O. Hellwig, *Phys. Rev. B* **2005**, *72*, 052410.
[35] D. M. Silevitch, T. F. Rosenbaum (University of Chicago), G. Aeppli, (University College London) "System and Method for Manipulating Domain Pinning and Reversal in Ferromagnetic Materials." U.S. Patent #8,558,333; EU Patent Application #10797895.9EPO 2013.